Enhanced Electrocatalytic Performance of Processed, Ultrathin, Supported Pd–Pt Core–Shell Nanowire Catalysts for the Oxygen Reduction Reaction

Christopher Koenigsmann,[†] Alexander C. Santulli,[†] Kuanping Gong,[‡] Miomir B. Vukmirovic,[‡] Wei-ping Zhou,[‡] Eli Sutter,[§] Stanislaus S. Wong,*,[†,⊥] and Radoslav R. Adzic*,[‡]

[†]Department of Chemistry, State University of New York at Stony Brook, Stony Brook, New York 11794-3400, United States

[‡]Chemistry Department, Brookhaven National Laboratory, Building 555, Upton, New York 11973, United States

[§]Center for Functional Nanomaterials, Brookhaven National Laboratory, Building 735, Upton, New York 11973, United States

[⊥]Condensed Matter Physics and Materials Sciences Department, Brookhaven National Laboratory, Building 480, Upton, New York 11973, United States

Ⓢ *Supporting Information*

ABSTRACT: We report on the synthesis, characterization, and electrochemical performance of novel, ultrathin Pt monolayer shell—Pd nanowire core catalysts. Initially, ultrathin Pd nanowires with diameters of 2.0 ± 0.5 nm were generated, and a method has been developed to achieve highly uniform distributions of these catalysts onto the Vulcan XC-72 carbon support. As-prepared wires are activated by the use of two distinctive treatment protocols followed by selective CO adsorption in order to selectively remove undesirable organic residues. Subsequently, the desired nanowire core—Pt monolayer shell motif was reliably achieved by Cu underpotential deposition followed by galvanic displacement of the Cu adatoms. The surface area and mass activity of the acid and ozone-treated nanowires were assessed, and the ozone-treated nanowires were found to maintain outstanding area and mass specific activities of 0.77 mA/cm^2 and 1.83 A/mg$_{Pt}$, respectively, which were significantly enhanced as compared with conventional commercial Pt nanoparticles, core—shell nanoparticles, and acid-treated nanowires. The ozone-treated nanowires also maintained excellent electrochemical durability under accelerated half-cell testing, and it was found that the area-specific activity increased by ∼1.5 fold after a simulated catalyst lifetime.
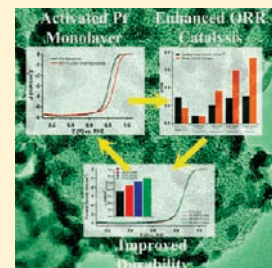
1. INTRODUCTION

Recent demand for low-cost, renewable energy has raised interest in terms of the commercial development of hydrogen-based polymer electrolyte fuel cells (PEMFCs).[1,2] Although PEMFCs are a promising future technology, a crucial limitation to the widespread application of PEMFCs has been the inherently slow oxygen reduction kinetics and a corresponding observed overpotential of the cathodic half cell.[3–6] The observed overpotential has been attributed in large part to the slow kinetics of oxygen reduction reaction (ORR) electrocatalysts, which consist primarily of platinum nanoparticles physisorbed onto mesoporous carbon supports.[7] A primary challenge with the use of nanoparticulate electrocatalysts for ORR is that these zero-dimensional (0D) morphologies possess proportionally higher numbers of defect sites, lattice boundaries, and low coordination atoms at their surfaces.[8] Inherently, defect sites are substantially less active towards ORR than defect-free crystal planes, largely because of differences in the local coordination geometry and surface energy, which can directly influence the interfacial interaction between the Pt surface sites and the adsorbed oxygen species.[1,9] In addition, defect sites are more readily passivated by the presence of adsorbed OH groups, which decrease the number of active Pt surface sites and inhibit catalysis at potentials below

1.0 V.[10] Not surprisingly, defect sites are also irreversibly oxidized more readily under operating potentials of 0.7 V, resulting in enhanced catalyst degradation, and thus, these 0D catalysts lack sufficient durability for long-term usage in practical, functional fuel cells.[5,11] These factors have culminated in the need for high precious metal loadings in the cathode of 0.15–0.25 mg/cm^2, which, as of 2009, represented ∼20% of the projected cost of a commercial fuel cell stack.[12]

Noble metal nanostructures possessing one-dimensional (1D) morphologies have been highlighted in the literature, as this structural motif may solve many of the inherent catalytic problems associated with state-of-the-art nanoparticulate catalysts. Recently, we have reviewed much of the literature on the rational development of one-dimensional nanostructure fuel cell catalysts, which have been demonstrated to possess enhanced electrocatalytic activity toward both ORR and methanol oxidation.[13] To summarize, 1D nanostructures are characterized by their uniquely anisotropic nature,[14] which imparts advantageous structural and electronic factors in the catalytic reduction of oxygen. For instance, the structural anisotropy of highly

crystalline 1D motifs results in the preferential exposure of low-energy crystalline planes so as to minimize the surface energy of the system.[15] In the case of platinum, the low energy (111) and (100) facets are most active toward ORR in perchloric acid solution, thereby making these anisotropic structures uniquely advantageous as ORR electrocatalysts.[16] Similarly, the preferential display of smooth crystalline planes minimizes the number of undesirable low-coordination defect sites, which is expected to enhance both ORR activity and long-term durability.[8,11,17] These factors are expected to culminate in the suppression of the cathodic overpotential by delaying surface passivation of adsorbed OH groups to higher potentials and thereby increasing the interfacial ORR kinetics.

Not surprisingly, there have been several reports in the literature highlighting the enhanced electrocatalytic ORR activity of one-dimensional noble metal nanostructures.[18–24] For instance, our group has recently prepared both 200 nm platinum nanotubes[23] and acid-treated ultrathin <2 nm platinum nanowires[19] utilizing optimized, ambient, surfactantless techniques. These as-prepared 200 nm nanotubes and <2 nm nanowires maintained area-specific activities of 0.38 and 1.45 mA/cm^2, which represent outstanding enhancements of 2-fold and 7-fold higher, respectively, than that of commercial carbon supported platinum nanoparticles. Interestingly, we observed a distinctive size-dependent enhancement in the area-specific ORR activity. Specifically, when the diameter is rationally decreased from 200 nm to the ultrathin size of ∼1 nm, the activity is increased by nearly 4-fold, which starkly contrasts with the observed trend associated with analogous platinum nanoparticles. It is believed that this size-dependent enhancement results from a characteristic contraction of the ultrathin platinum nanowire surface, which had been previously observed, both experimentally and theoretically. In addition, cyclic voltammetry and HRTEM characterization of as-prepared ultrathin nanowires revealed that they maintained fewer low coordination (defect) sites and possessed a surface that was analogous to that of a bulk Pt (111), which would also contribute to an enhancement in ORR activity. In another report, 3-fold enhancements in area-specific activity have been observed with platinum nanowires grown directly onto a carbon support.[21]

Although the enhancements in area-specific activity observed with one-dimensional nanostructures are promising, a continuing challenge with the development of electrocatalysts composed entirely of platinum has been the prohibitive cost associated with elemental platinum as well as its relatively low abundance. Hence, there has been significant effort recently expended toward the improvement of platinum mass activity by utilizing palladium and palladium-based alloys, many composed of one-dimensional morphologies, as suitable replacements.[18,20,25] Recently, Abruña and co-workers[25] have observed similar structure-dependent enhancement in ORR activity with palladium-based nanorod catalysts prepared by electrodeposition directly onto a carbon support. Utilizing a combinatorial approach, the enhanced activity in this case was attributed to the preferential display of certain low energy crystal facets, which have been predicted by DFT to be most active toward ORR in the case of Pd. Despite the significantly enhanced activity, the activity of these as-prepared nanorods did not surpass the activity of bulk platinum, which is largely considered to be one of the most active surfaces for ORR. In another report, Yan and co-workers[18] prepared polycrystalline PtPd nanotubes, which maintained a 1.4 fold higher mass activity of approximately 0.1 A/mg$_{Pt}$ at 0.85 V as compared with

commercial platinum black catalysts. Similarly, Xia and co-workers have recently observed a degree of enhancement in mass activity of isotropic Pt dendrites, grown directly onto Pd nanoparticles.[20] Despite these tangible gains, continued improvement is necessary in order to meet the 2015 U.S. Department of Energy (DOE) target[26] for performance in an oxygen reduction environment under membrane electrode assembly (MEA) conditions, namely a platinum mass activity of 0.44 A/mg (at 0.9 V).

A promising route toward improving platinum mass activity, that has achieved considerable attention recently, has been the development of Pd nanocrystals possessing a Pt monolayer shell, a strategy pioneered by one of our groups.[27–30] The highly controlled core–shell structure in this case has been achieved by first electrochemically depositing a monolayer of Cu atoms through the use of Cu underpotential deposition (UPD) followed by the controlled displacement of these adatoms with platinum via galvanic exchange.[31] In a recent report, the activity of the optimized Pt monolayer supported onto commercial Pd nanoparticles was studied systematically, and as-prepared catalysts were found to have outstanding mass and area-specific ORR activities of 0.96 A/mg$_{Pt}$ and 0.5 mA/cm^2, respectively.[32] The significant enhancements in activity have been attributed to the uniquely advantageous core–shell motif, which modifies both the structural and electronic properties of platinum for enhanced activity. Specifically, the Pd substrate is thought not only to apply a compressive strain upon the Pt monolayer but also to impart a so-called "ligand-effect", representing phenomena which have mutually been found to lower the energy of the weighted center of the Pt d-band. The resulting suppression of the Pt d-band energy is thought to directly provide for a weakened interaction with OH$_{ads}$ groups, thereby yielding improved ORR activity.[33,34]

Although outstanding results have been achieved with 0D core–shell catalysts based upon the platform of commercial Pd nanoparticles, to the best of our knowledge, there have been no reports on the structural and morphological dependence of ORR activity in catalysts bearing this unique core–shell motif. Hence, in this paper, we combine the uniquely advantageous core–shell motif with the known electrocatalytic advantages of ultrathin one-dimensional nanostructures in order to rationally enhance the activity and durability of the resulting catalyst. Specifically, the use of ultrathin nanowires with diameters below 5 nm maximizes the surface area-to-volume ratio, and therefore higher mass activities can be achieved. More importantly, noble metal nanowires have been shown both theoretically[35,36] and experimentally[37] to undergo a distinctive surface contraction when their diameter is decreased below a critical value of 2 to 3 nm. A contraction of the core nanowire surface would be highly advantageous for ORR electrocatalysis, because this would enhance the strain induced contraction of the Pt monolayer and therefore augment the inherent ORR activity.

In this report, we first discuss the synthesis and characterization of ultrathin ∼2 nm Pd nanowires supported onto conductive carbon supports (Pd NW/C), utilizing a surfactant-based synthetic technique coupled with a novel methodology for supporting these as-prepared nanowires. Subsequently, the as-prepared Pd NW/C composites are processed, utilizing two separate and independent treatments in order to electrochemically activate the nanowires by removing residual undesirable surfactant. The impact of these diverse treatment protocols upon the electrochemical properties of the nanostructures has been analyzed. It is critical to highlight that, to the best of our knowledge,

9784

dx.doi.org/10.1021/ja111130t |J. Am. Chem. Soc. 2011, 133, 9783–9795

there have been no previous reports of either supported or activated ultrathin Pd nanowires with a diameter of less than 5 nm. We then rationally explore the structure-dependent enhancement of ORR activity of as-prepared ultrathin Pd nanowires by comparison with commercial carbon-supported Pd nanoparticles. Ultimately, the desired Pd nanowire core—Pt monolayer shell structure can be prepared by utilizing Cu UPD followed by galvanic displacement. Hence, the novelty of this report is 3-fold: (i) this is, to the best of our knowledge, the first report of activated ultrathin Pd nanowires reliably supported on high surface area carbon; (ii) a new methodology has been outlined wherein both wet techniques and a novel electrochemical technique, i.e., selective carbon monoxide (CO) adsorption, are employed in tandem to activate as-prepared nanowires; and (iii) the structure dependence of ORR in core—shell Pt monolayer catalysts has been explored for the first time. Specifically, the size-dependent enhancement of both area and mass-specific activity has been investigated herein. We find that the ozone-treated Pd NW core—Pt monolayer shell nanostructures maintain a platinum mass activity of 1.83 A/mg, which is more than double that associated with optimized core—shell catalysts based upon nanoparticle motifs.

2. MATERIALS AND METHODS

2.1. Synthesis of Pd NW/C Composites. Initially, unsupported ultrathin Pd nanowires were prepared, utilizing a modified procedure previously reported by Teng et al.[38] Briefly, palladium nitrate (13.0 mg, Alfa Aesar 99.9%), octadecylamine (400 mg, Acros Organics 90%), and dodecyltrimethylammonium bromide (60 mg, TCI >99%) were dissolved in 7 mL of toluene under vigorous magnetic stirring. The mixture was brought under an inert atmosphere, utilizing standard Schlenk procedures, and was sonicated for 20 min. Separately, solid sodium borohydride (13 mg, Alfa Aesar 98%) was dissolved into 2 mL of deoxygenated distilled water, and the solution was added dropwise to the precursor mixture, while stirring. After 1 h, the reaction mixture was diluted with 2 mL aliquots of distilled water and chloroform, resulting in the separation of the organic and aqueous phases. The black organic phase was isolated, diluted with 10 mL of absolute ethanol, and centrifuged for 10 min, thereby resulting in the precipitation of a black solid. The black solid was subsequently washed several times with ethanol and allowed to dry in air.

Adsorption of these as-prepared nanowires onto conductive carbon support (Vulcan XC-72, Cabot) was achieved by first dispersing the isolated black solid containing a mixture of Pd nanowires and residual surfactant into 6 mL of chloroform, until a homogeneous black mixture was formed. An equal mass of Vulcan carbon (~6 mg) was then added to this mixture, and the mixture was subsequently sonicated for 30 min in a bath sonicator. As-prepared composites were then isolated by centrifugation and fixed onto the carbon substrate by immersion in hexanes for 12 h. After being washed several times with hexanes and ethanol, as-prepared composites were further cleansed with either hexane or acetone in order to remove residual surfactants prior to drying overnight.

2.2. Activation of Pd/C NW Catalysts. Three separate protocols were utilized in order to activate the as-prepared catalysts and to suitably remove the residual surfactant. First, we utilized a heat treatment process wherein the Pd NW/C powder was heated to 250 °C in air for 1.5 h within a muffle furnace. The heat-treated powder was then dispersed in ethanol for the purposes of electron microscopy. Second, an acid wash protocol previously described for Pd nanoparticles[39] was suitably optimized for use with Pd nanowire samples, so that the desired 1D morphology could be maintained. Dried, as-prepared catalyst powder was dispersed in 5 mL of glacial acetic acid by bath sonication for 30 min within a fume hood. The mixture was then brought to 50 °C for 1 h, the

mixture was centrifuged while still hot, and the acetic acid was later decanted. The treated composites were then washed several times with ethanol and allowed to dry overnight. After treatment, a catalyst ink was prepared by adding an appropriate amount of 25% isopropyl alcohol (IPA) solution to the dry powder so as to provide for a 2 mg/mL concentration. The catalyst powder was suitably dispersed into the ink by sonication for 45 min to achieve a uniform distribution. Third, we utilized a novel time-controlled UV—ozone treatment. In this case, dried, as-prepared catalyst powder was dispersed into ethanol by sonication after which several drops were placed onto a silicon wafer. The wafers were placed into a UV—ozone generator (UVOCS model no. T10X10-0ES) and treated for 15 min. As-treated nanowires were then isolated from the wafers by sonication into a 25% IPA solution, thereby ultimately yielding the final catalyst ink solution of approximately 1 mg/mL.

2.3. Characterization. The X-ray diffraction work was performed on a Scintag diffractometer, operating in the Bragg—Brentano configuration using Cu Kα radiation (λ = 1.54 Å) at a scan rate of 0.2° in 2θ per minute. Powder diffraction samples were prepared by rendering the dried powders into slurries in ethanol after sonication for several minutes. The slurries were then air-dried onto glass slides.

The morphology of the catalyst composites was characterized initially with low magnification transmission electron microscopy (TEM) images taken at an accelerating voltage of 80 kV on a FEI Tecnai12 BioTwinG^2 instrument, equipped with an AMT XR-60 CCD Digital Camera System. High-resolution TEM (HRTEM) images and selected area electron diffraction (SAED) patterns were obtained on a JEOL 2010F instrument, equipped with a Gatan high-angle annular dark field detector (HAADF) for performing either incoherent HAADF or Z-contrast imaging in scanning TEM mode at accelerating voltages of 200 kV. Specimens for all of these TEM experiments were prepared by diluting the catalyst ink with ethanol, sonicating for 2 min in order to ensure adequate dispersion of the nanostructures, and evaporating one drop of the solution onto a 300 mesh Cu grid, coated with a lacey carbon film. Scanning electron microscopy (SEM) images were obtained by utilizing a field emission scanning electron microscope (Hitachi S-4800), operating at an accelerating voltage of 15 kV. SEM samples were prepared by dispersing in ethanol and sonicating for several minutes, followed by drop-casting onto a silicon wafer.

Thermogravimetric analysis of the various dry catalyst powders was performed on a TGA Q500 (TA Instruments). Isotherms were obtained by raising the temperature from 25 to 900 °C at a rate of 10 °C/min under a flow of ultradry high purity air, provided at a rate of 60 mL/min. The mass profiles reveal that the decomposition of the carbon is initiated at ~300 °C and is complete by 600 °C. The weight percent of palladium can be obtained after 800 °C, wherein all carbonaceous material has been removed. The palladium loading was found to be 29.6% for the untreated sample, and it increased slightly to 31.4% and 36.9% after ozone and acid treatment, respectively. The slight increase in the palladium weight percent can be attributed to loss of residual surfactant and carbon after treatment. The palladium mass loading was also independently verified by performing TGA analysis on 30 μL of the catalyst ink used in the electrochemical experiments and dried directly in the platinum pan.

2.4. Deposition of Pt Monolayer Shell. The deposition of the platinum monolayer shell was accomplished utilizing a method pioneered by one of our groups.[30,31] Briefly, a 5 μL drop of the appropriate catalyst ink was placed onto a polished glassy carbon electrode (GCE) (RDE, Pine Instruments, 5 mm active area) and allowed to air-dry, thereby forming a uniform catalyst layer. For all electrochemical measurements, a reference electrode (Ag/AgCl, 3 M Cl$^-$) was used with a double-junction chamber (Cypress) and platinum foil served as the counter electrode. All of the potentials recorded in this paper are given with respect to a reversible hydrogen electrode (RHE), unless otherwise stated. Before deposition, residual surfactant was removed

9785

dx.doi.org/10.1021/ja111130t |*J. Am. Chem. Soc.* 2011, 133, 9783–9795

from the surface of the treated Pd catalyst by displacement of the surface ligand with CO followed by CO stripping. Adsorption of CO was achieved by immersing the electrode in a CO-saturated 0.1 M $HClO_4$ solution under a CO blanket for 30 min. The electrode was transferred to a fresh electrolyte, and the adsorbed CO was subsequently stripped from the surface by a potential sweep, running up to 1.1 V at 20 mV/s. A monolayer of Cu was then deposited by Cu UPD from a deoxygenated solution of 50 mM $CuSO_4$, maintained in a 0.10 M H_2SO_4 electrolyte.[32] The Cu monolayer modified electrode was transferred to and immersed in a solution of a 1.0 mM K_2PtCl_4 solution in 50 mM H_2SO_4 for several minutes. All of these steps were performed in a custom-made two-chamber electrochemical apparatus, which allows for the transfer of the Cu monolayer modified electrode under an inert Ar atmosphere, so as to protect the Cu adatoms from oxidation. The Pt monolayer modified electrode was removed from the cell and rinsed thoroughly, before being covered by a 5 μL drop of Nafion solution (0.025% in ethanol), which had been prepared from an initial 5% stock solution (Aldrich).

2.5. Measurement of ORR Activity and Catalyst Durability.
Studies of the kinetics of ORR on both 1-D nanowire and commercial nanoparticle catalysts have been performed using the thin-layer rotating disk electrode (RDE) method.[40] Specifically, cyclic voltammetry was performed in a deoxygenated 0.1 M $HClO_4$ solution with a scan rate of 20 mV/s. Polarization curves were obtained in O_2-saturated 0.1 M $HClO_4$ solutions at 20 °C with a scan rate of 10 mV/s and a rotation rate of 1600 rpm. The ORR activity of the as-prepared activated Pd NW/C and Pt monolayer–Pd NW/C catalysts was compared with that of commercial Pd and Pt nanoparticles, respectively, adsorbed onto Vulcan XC-72 carbon (20% by weight of total Pt metal, E-tek) and rendered into 2 mg/mL catalyst inks in 25% IPA. The durability testing of both as-prepared and commercial catalysts was performed under half-cell conditions in perchloric acid, utilizing a durability test protocol described by the U.S. DOE for simulating a catalyst lifetime under MEA conditions.[26] Specifically, the potential was cycled from 0.6 to 1.0 V in 0.1 M $HClO_4$ and left open to the atmosphere. The electrochemical surface area (ESA) was obtained after every 5000 cycles, and the electrochemical surface area activity was measured after every 10 000 cycles. For the durability tests, the durability of the nanowires was compared with high performance (HP) Pt nanoparticles adsorbed onto Vulcan XC-72 carbon (20% by weight of total Pt metal, E-tek).

3. RESULTS AND DISCUSSION

3.1. Synthesis and Characterization of Pd NW/C. The synthesis of the Pd nanowire core in this case was readily achieved by utilizing a surfactant-based method[38] wherein the reduction of Pd^{2+} is directed by the surfactant agent, ocatadecylamine (ODA). The crystallinity and purity of the subsequent as-prepared nanowires was verified using X-ray powder diffraction (XRD). The crystallographic analysis (Figure S1A, Supporting Information) revealed that all of the peaks could be readily attributed to the (111), (200), (220), and (311) reflections of face-centered cubic palladium ($Fm3m$, JCPDS no. 46-1043). There were no detectable crystalline impurities observed in the XRD pattern. The morphology of as-prepared Pd NWs was initially characterized by electron microscopy. An overview TEM image presented in Figure S1B revealed that as-prepared nanowires maintained ultrathin diameters of 2.0 ± 0.5 nm with average lengths in excess of 100 nm. High resolution SEM images (inset to Figure S1B) confirmed the inherent quality and dimensions of as-prepared Pd NWs. However, it was apparent that there was still a substantial undesirable surfactant residue present, despite multiple washes with ethanol. Upon the basis of the high solubility of ODA in chloroform,[41] as-prepared

nanowires were washed multiple times with chloroform in order to remove the residual surfactant. However, overview TEM images (Figure S2, Supporting Information) of the chloroform-washed product revealed that the nanowires became heavily agglomerated and the nanowire morphology was lost. Similarly, rapid agglomeration was observed after washing with other solvents, including dimethylformamide (DMF) and toluene.

Hence, a methodology was developed so as to reproducibly immobilize the as-prepared nanostructures onto a conductive carbon support in order to prevent rapid agglomeration upon removal of the surfactant. Conductive carbon supports are ubiquitous in nanostructured catalyst design, because they impart excellent durability to the supported nanostructures, slow Oswald ripening processes under applied potential, and increase the conductivity of the catalyst layer in working fuel cells.[42] In addition, the high degree of dispersion that can be achieved with nanostructures supported on carbon has been previously shown to enhance the mass activity of catalysts.[43] A critical element in the process of supporting nanostructures is the determination of an optimum solvent, i.e., chloroform, so as to maximize the dispersibility and uniformity of the catalyst onto the surface of the conductive carbon support. In fact, the as-prepared nanowires remained dispersed in chloroform for up to several months, whereas in other solvents, such as water and ethanol for instance, precipitation and agglomeration occurred, essentially overnight. Adsorption onto commercial carbon was achieved by a brief period of sonication with both components mutually dispersed in chloroform followed by centrifugation. Subsequently, the precipitated composites were dispersed into hexanes overnight in order to remove excess surfactant and affix the nanowires onto the carbon surface.

Interestingly, the aforementioned hexane wash was critical in achieving sufficient adsorption of the nanowires to the carbon. When the hexane washing step was excluded and the solid was dispersed into ethanol, the isolated product was found by TEM to contain agglomerates of Pd NWs and bare carbon. By contrast, the Pd NW/C composites isolated after immersion in hexanes for 24 h could be redispersed in a broad range of solvents with sonication without either any apparent desorption or aggregation of the nanowires. We attribute this effect to the rapid solubilization of excess ODA during the hexane washes. Upon the basis of the agglomeration of the unsupported nanowires when immersed in hexanes, it is believed that the hexane wash contributes to a partial desorption of the ODA from the Pd NW surface, thereby resulting in aggregation. Similarly, it has been reported that hexanes in combination with ethanol can suitably expose the surface of Pd nanoparticles capped with oleylamine, an analogous surfactant.[44] Hence, it is not surprising that the hexane wash of the Pd NW/C results in the partial solubilization of ODA from the Pd NW and the carbon surfaces, thereby strengthening the interaction between the Pd and the carbon.

The structure and crystallinity of the Pd NW/C composites were studied by XRD and electron microscopy. The XRD pattern shown in Figure 1A of the Pd NW/C revealed that the adsorption process had no effect upon the purity and crystallinity of the sample, because all of the peaks could again be readily indexed to the (111), (200), (220), and (311) reflections of the face-centered cubic palladium phase. An overview TEM image (Figure 1C) of the composites revealed that the nanowires largely maintained their wire-like morphology as well as their dimensionality, e.g., their ultrathin diameter of approximately 2 nm (2.2 ± 0.5 nm). However, a small percentage (~5%) of
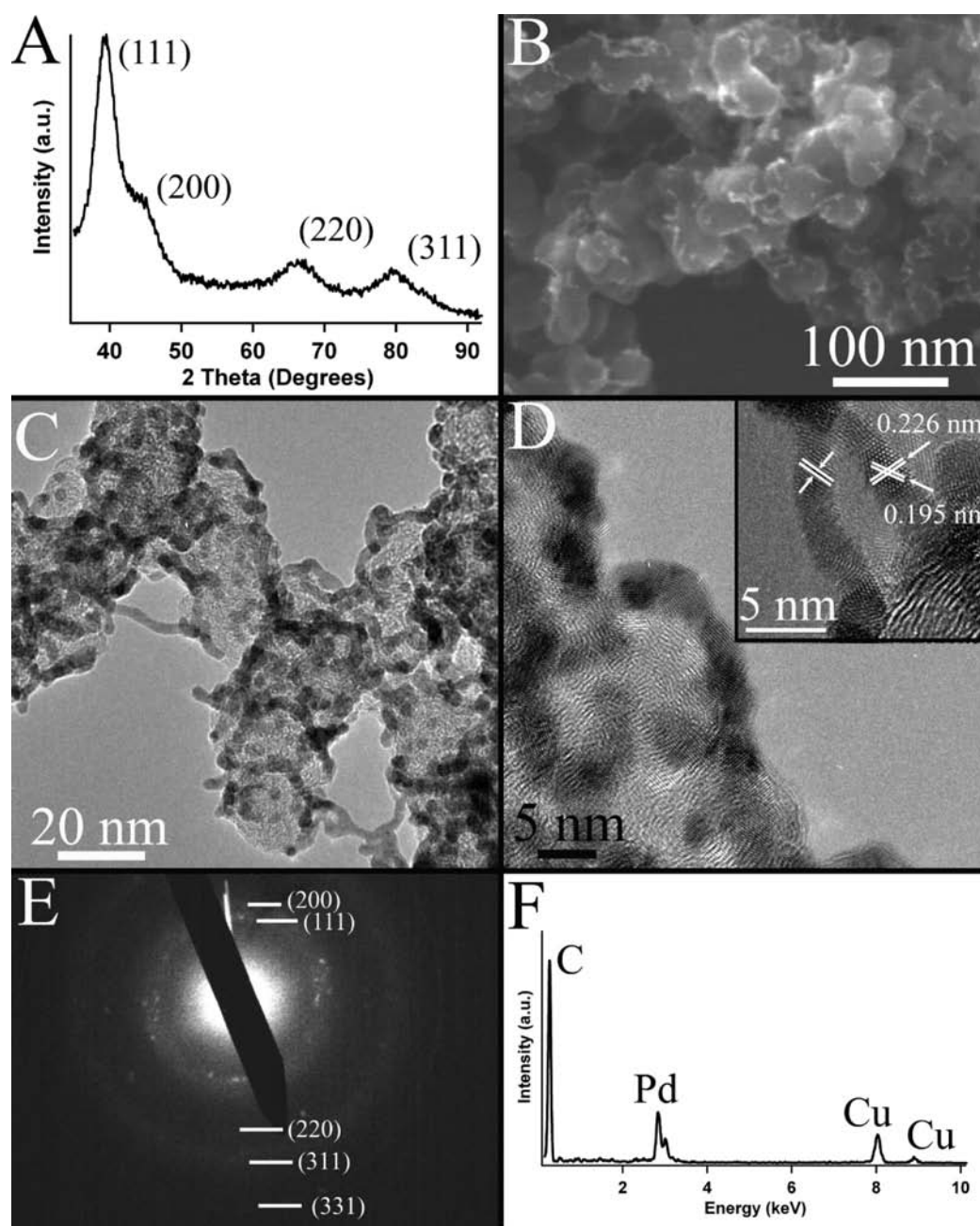
Figure 1. Representative experimental powder XRD pattern (A) of as-prepared Pd NW/C composites. Overview FESEM (B) and low resolution TEM (C) of as-prepared Pd NW/C composites. A high-resolution TEM image of single palladium nanowires is shown as an inset within an image (D) of a representative collection of these nanowires. Associated selected area electron diffraction (E) and energy dispersive X-ray spectroscopy (F) of the Pd NW/C composites.

nanoparticles was apparent. The supported wires possessed measurably smaller lengths as compared with as-prepared nanowires, with lengths estimated to be only up to 30 nm. Indeed, FESEM (Figure 1B) images further confirmed the presence of Pd NWs adsorbed onto the carbon surface and also revealed that a uniform distribution of catalyst could be achieved. The presence of nanoparticles and the observed decrease in nanostructured length could be readily attributed to the effect of the mechanical stress associated with sonication of the nanowires in the presence of the carbon support.

Upon the basis of the high resolution TEM (HRTEM) shown in Figure 1D, the nanowires are polycrystalline and are composed of multiple single crystalline segments with lengths of 6 ± 1 nm, that extend along the axis of the nanowire. Not surprisingly, the single crystalline segments making up the nanowires possess lattice spacings of 0.226 and 0.195 nm, consistent with (111) and (200) lattice spacings, respectively. The selected area electron diffraction (SAED) pattern shown in Figure 1E highlights the presence of not only continuous rings that can be indexed to palladium's (111), (200), (220), (311), and (331) planes, respectively, but also discrete diffraction spots, indicating that
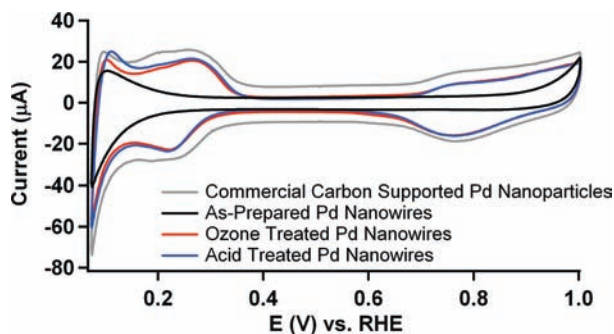
Figure 2. Cyclic voltammograms obtained for the carbon-supported ozonized and acid-treated nanowires after selective CO adsorption and CO stripping, shown by comparison with an as-prepared nanowire sample and commercial carbon-supported Pd, loaded separately onto a GCE in a deoxygenated 0.1 M $HClO_4$ solution at 20 mV/s.

the high degree of crystalline substructure observed is representative of the whole ensemble of nanowires that contributed to the observed diffraction pattern. The composition of individual nanowires was investigated using energy dispersive X-ray spectroscopy (Figure 1F) in scanning TEM mode with an electron beam size of 0.2 nm and highlights only the elemental presence of Pd and C, with the Cu peaks emanating from the TEM grid.

3.2. Activation of Pd NW/C for Effective Electrocatalysis. The electrochemical performance and surface contamination of as-prepared Pd NW/C composites were initially studied by cyclic voltammetry in order to determine if residual organic residues were present on the surface of the nanowires. Specifically, cyclic voltammograms obtained in 0.1 M $HClO_4$ solution (Figure 2) revealed that the surface of the Pd NWs was entirely passivated by residual surfactant, despite the ethanol and hexane washes. By comparison with commercial carbon-supported Pd nanoparticles, the Pd NW/C composites showed an almost complete suppression of the hydrogen adsorption (H_{ads}) peaks in the region of 0−0.35 V and a delay in the formation of the oxide region to almost 0.9 V, thereby confirming that the active surface sites were not readily accessible to the electrolyte.

In order to suitably expose the Pd surface, we utilized a novel method that combines selective CO adsorption with either an acid treatment or a UV-generated ozone treatment in order to remove the undesirable organic residue and electrochemically activate the Pd nanowires without structurally compromising the uniquely advantageous one-dimensional structure. This is the first report wherein the adsorption of CO is utilized as a reliable method for removing surfactant. Desorption of the coordinated organic molecules is accomplished by first weakening the interaction of the surfactant to the surface either by acid or ozone treatment. This step is followed by the preferential adsorption of a CO monolayer, which strongly coordinates[45,46] to the surface of noble metals under slightly reducing potentials and displaces undesirable organic residues. Subsequently, the pristine surfaces of the catalyst can be readily exposed by electrochemical oxidation of the CO monolayer (CO stripping).

Initially, the as-prepared Pd NW/C composites were supported onto a GCE and selective adsorption of CO was attempted in a CO saturated 0.1 M $HClO_4$ solution under reducing potentials. However, the cyclic voltammogram (Figure S4, Supporting Information) remained unchanged despite more than 2 h of immersion in the CO saturated solution. The absence of any change in the cyclic voltammogram was a

clear indication that the residual ODA on the surface sufficiently blocked the adsorption of CO. In this case, the strong adsorption of the amine functional group to the surface of Pd and the inherent hydrophobicity of the alkyl chain present in ODA prevent effective adsorption of CO from the solution. Not surprisingly, a previous study has shown that Pd nanoparticles when capped with an analogous amine-terminated dendrimer chain prevented effective heterogeneous catalysis of the Suzuki reaction.[47] By contrast, the Suzuki reaction was not hindered by the presence of other surfactants such as polyvinyl pyrrolidone (PVP) and certain block copolymers. It is believed that the strong interaction between the terminal amine functionality and the Pd surface in combination with the strongly hydrophobic end groups of the adsorbed surfactant (i) blocks the active Pd surface sites and (ii) prevents effective transport of reactants onto the surface of Pd.

In order to suitably remove the surfactant, we utilized two separate treatment protocols so as to weaken the interaction of the ODA with the surface of the Pd NWs and thereby enhance the selective adsorption of CO. The first treatment method involves the use of an acid wash protocol previously utilized for oleylamine-capped Pd nanoparticles[39] that has been suitably optimized in order to maintain the one-dimensional morphology of our as-prepared catalysts. Acid treatments are widely utilized in nanomaterial purification, particularly in the treatment of carbon nanotubes[48] and plasma etched thin films[49] of noble metals. In a recent report, our group has utilized a novel acid treatment in order to purify analogous ultrathin Pt nanowires. As-treated nanowires displayed a surface area activity for ORR that was more than 3-fold higher as compared with untreated nanowires.[19] In this report, the Pd NW/C composites are processed in glacial acetic acid for 1 h at elevated temperatures in order to suitably destabilize the interaction between the ODA and the Pd surface. Overview TEM and SEM images of the acid-treated Pd NW/C are shown in Figure 3, parts A and B, respectively. Treated Pd nanowires possess a largely one-dimensional morphology and the ultrathin diameter of 2.3 ± 0.5 nm was maintained. However, it is apparent from both TEM and SEM images that the acid treatment results in significant aggregation of the nanowires into net-like bundles and that there was also a noteworthy increase in the fraction of nanoparticles present, to approximately 10−15%.

Interestingly, cyclic voltammetry of the acid-treated Pd NW/C obtained after selective CO adsorption followed by CO stripping (Figure 2) displayed both characteristic H_{ads} peaks in the region of 0 to 0.2 V and the onset of oxide formation at ∼0.7 V. The strong similarity between the voltammetric response of the acid-treated Pd NW/C composites and that of commercial carbon-supported Pd nanoparticles confirmed that the surfactant had been successfully removed from the surface. In previous reports, both organic and inorganic acids have been found to weaken the interaction of amine-based surfactants with Pd nanoparticles at pH values of less than 2 by collectively contributing to the protonation of the amine functional group and an increase in the ionic strength of the solution.[39,47] Thus, we believe that the suppression of the ODA−Pd interaction by the acid treatment contributes to an enhancement in the selective adsorption of CO and the inevitable displacement of the surfactant.

The second treatment involves the time-controlled exposure of the Pd NW/C composites to UV-generated ozone. Recently, UV−ozone has been successfully utilized to remove amine-terminated surfactants from both Pt[50] and Au[51] nanoparticle
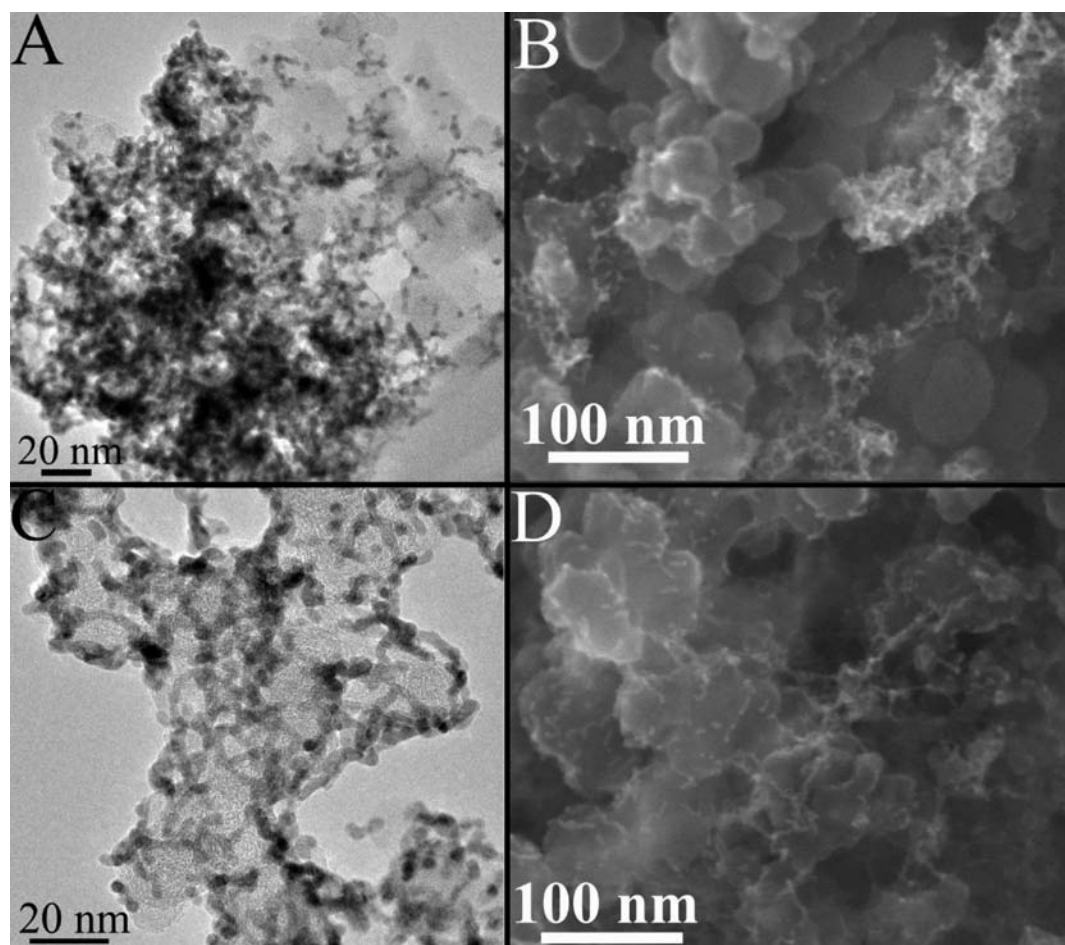
Figure 3. Representative TEM (A and C) and SEM (B and D) images of supported Pd NW/C composites after treatment in acid (A and B) and UV-generated ozone (C and D), respectively.

monolayers supported on solid substrates. However, there have been a number of mixed results with respect to the effectiveness of UV–ozone for activating capped nanoparticles for use as electrocatalysts.[52−54] In one report, UV–ozone was successfully utilized to remove the residual organic residue present on a monolayer of unsupported FePt nanoparticles deposited on a Au electrode substrate, which had been used to activate as-prepared nanoparticles toward formic acid oxidation.[55] By contrast, a recent report from Nikles and co-workers suggested that UV–ozone was not as effective in removing an amine-terminated surfactant, analogous to ODA, from Pt nanoparticles supported on commercial Vulcan carbon.[53,56]

In this report, we utilized a short 15 min UV–ozone treatment in order to suitably weaken the interaction between the residual ODA and the surface Pd, thereby allowing for effective removal of the ODA by selective CO adsorption. Representative overview TEM and SEM images of the Pd NW/C composites after UV–ozone treatment are shown in Figure 3, parts C and D, respectively. By comparison with the electron microscopy data associated with untreated samples, the ozone treatment does not contribute to any significant change in either the morphology or distribution of as-prepared Pd NW/C. Upon the basis of the TEM images, the ozone-treated nanowires largely retain the desirable one-dimensional, wire-like morphology. However, there is some fragmentation of the nanowires resulting in the

presence of short wire fragments as well as some nanoparticles. Nevertheless, the SEM images of ozone-treated nanowires, which show a broader perspective, confirm the presence of a majority of long nanowires and nanowire fragments with some nanoparticles present. There is no significant change in the reported ultrathin diameter of 2.2 ± 0.8 nm. By contrast with the acid-treated samples, the ozone-treated samples maintain a high degree of dispersion on the carbon substrate, and there is little appreciable aggregation. Overview SEM images, which provide a more representative view of a thin catalyst layer, highlight the presence of longer nanowires with lengths in excess of 100 nm that are apparent on larger carbon aggregates and short wire-like fragments with average lengths of 26 ± 11 nm.

After ozone treatment, the Pd NW/C composites were deposited onto a GCE, and selective CO adsorption was performed in order to remove the residual surfactant. After CO stripping, cyclic voltammograms (Figure 2) of the Pd NW/C composites showed H_{ads} and oxide formation features that were in excellent agreement with the commercial Pd NPs, thereby confirming that the surfactant was removed. More importantly, the H_{ads} profile of the ozone-treated composites is in excellent agreement with that of the acid-treated composites, which clearly demonstrates that both methods are equally effective at removing the residual surfactant. Based upon the aforementioned reports, the formation of gaseous ozone, a weak oxidizing agent,
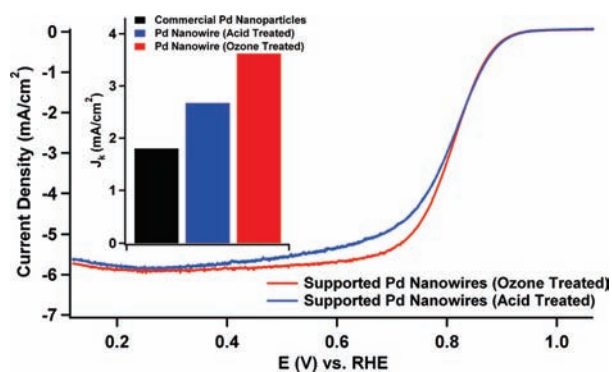
9789

dx.doi.org/10.1021/ja111130t |*J. Am. Chem. Soc.* 2011, 133, 9783–9795

Figure 4. Polarization curves for treated Pd nanowire samples immobilized onto a glassy carbon rotating disk electrode. Curves (anodic sweep direction) were obtained with a rotation rate of 1600 rpm in a 0.1 M $HClO_4$ solution at 20 °C. Electrochemical surface area activities (inset) at 0.8 V for variously treated Pd nanowire samples, shown by comparison with commercial supported Pd nanoparticles.

is thought to oxidize the organic molecules, coating the nanocrystals, thereby forming volatile carbon and nitrogen compounds.[51,55] However, the complete volatilization of long-chain amine-terminated compounds may require up to several hours of exposure, which may result in an unwanted oxidation of the nanoparticle.[50] In our case, we utilized a short treatment time of 15 min to only partially oxidize the carbon chain and, more importantly, the terminal amine functional group, so as to weaken the interaction of the ODA with the surface. Thus, by suitably oxidizing the terminal amine functional group, the interaction between the ODA and the Pd surface can be sufficiently reduced so as to allow for enhanced adsorption of CO to the surface.

A critical aspect of these treatment protocols is that the single crystalline segments are maintained despite some fragmentation and aggregation. These single crystalline segments represent the key structural unit of the nanowires because they are expected to possess the most electrocatalytically active surface sites for ORR. To highlight the importance of the aforementioned techniques in maintaining the desired one-dimensional morphology, we also utilized two protocols that are commonly meant to remove organic residues from nanoparticulate catalysts.[57] First, we undertook thermogravimetric analysis (TGA) to rationally design a heat treatment protocol so as to thermally desorb the ODA from the Pd surface. Upon the basis of TGA isotherms, the Pd NW/C powder was heated to 250 °C in air or in nitrogen for 1.5 h in order to completely remove the undesired organic residue. Second, we also utilized cyclic voltammetry, wherein the potential was cycled to ∼1.65 V vs RHE, so as to selectively oxidize the amine functional group of the ODA and thereby expose the catalyst surface. However, representative TEM images of the products isolated after these two traditional treatment protocols (Figure S3, Supporting Information) showed complete conversion of the nanowires to nanoparticle aggregates. Hence, effective protocols conventionally utilized for the activation of nanoparticulate catalysts cannot be blindly applied to 1D catalysts with the expectation of a conservation of morphology. More importantly, this system of methodologies highlights the versatility of selective CO adsorption, wherein undesirable organic residues can be removed without the need for harsh reaction conditions, which can be structurally detrimental to nanostructures

with 1D morphologies and their correspondingly small diameters.

3.3. Structure-Dependent ORR Activity of Pd NW/C Composites. Initially, the electrochemical surface area (ESA) of nanowire and commercial nanoparticle catalysts was determined by integration of the CO stripping peak shown in Figure S5, Supporting Information. We elected to utilize the CO stripping charge (cf., Supporting Information) in the case of the Pd nanostructures because it is widely known that the H_{ads} profile is unreliable as a result of substantial hydrogen absorption.[58] Subsequently, the ORR activity for the treated Pd NW samples was measured electrochemically by obtaining polarization curves (Figure 4) in an oxygen-saturated 0.1 M $HClO_4$ solution. The nanowire samples show an ORR onset between 0.85 and 0.9 V, which is consistent with that of nanostructured Pd catalysts. More importantly, the measured kinetic currents at 0.8 V were normalized to the ESA (inset to Figure 4) so as to probe the intrinsic activity of the catalysts. In this case, we have elected to measure the kinetic current at 0.8 V, because the Pd-based catalysts show almost no activity at 0.9 V. On the basis of this protocol, the ozone-treated nanowires displayed an electrochemical surface area activity (ECSA) of 3.62 mA/cm^2, which was approximately 1.4 fold higher as compared with that of acid-treated nanowires (2.67 mA/cm^2).

We attribute the higher activity in the ozone-treated nanowires to the uniquely advantageous nature of the ozone treatment. From a structural perspective, the key structural unit of these nanowires consists of the elongated single crystalline segments that compose the wires. Although both treatment protocols preserve these elongated single crystalline segments, the primary difference is that the ozone-treated nanowires maintained (i) an improved dispersion of the wires on the carbon, (ii) less aggregation of the wires during processing, and (iii) the formation of fewer nanoparticles, as compared with the acid-treated nanowires. As expected, the structure of the polarization curve in the mixed control region indicates that the ozone-treated nanowires maintain an improved dispersion on the carbon coupled with less aggregation.[1,59] As we have previously shown, highly dispersed ultrathin nanowires, possessing certain pristine, defect-free surfaces, are significantly more active toward ORR, as compared with analogous aggregated nanowires.[19] Interestingly, this observed difference in the kinetic current at 0.8 V highlights the importance of treatment protocols. In fact, there is a clear correlation between structure and the resulting activity of the as-generated catalysts.

In addition to observing a treatment-dependent ORR activity, the nanowires also showed a distinctive structure-dependent enhancement, when the catalytic activity of the nanowires was compared with that of commercial Pd nanoparticles. In fact, the ozone and acid-treated Pd NW/C samples showed a greater than 2 fold and 1.5 fold higher activity, respectively, as compared with the activity of commercial Pd NP/C composites (1.8 mA/cm^2). Not surprisingly, the 1D nanostructures displayed significantly enhanced activities, which can be attributed in part to their uniquely advantageous anisotropic structure.

In particular, 1D nanostructures preferentially display smooth, low energy crystal facets, which maintain fewer defect sites as compared with analogous nanoparticulate catalysts.[13] Previously, we have prepared ultrathin Pt nanowires within basic media, which maintained relatively few defect sites. These possessed low energy crystalline facets and a corresponding ⟨111⟩ growth direction, based on CV and HRTEM results. These ultrathin

Figure 6. The electrochemical surface area activity (ECSA, mA/cm^2) and the mass activity (A/mg) at 0.9 V for the Pt−Pd nanowire samples are shown by comparison with commercial carbon-supported Pt nanoparticles along with the reported values for optimized Pt−Pd nanoparticles.
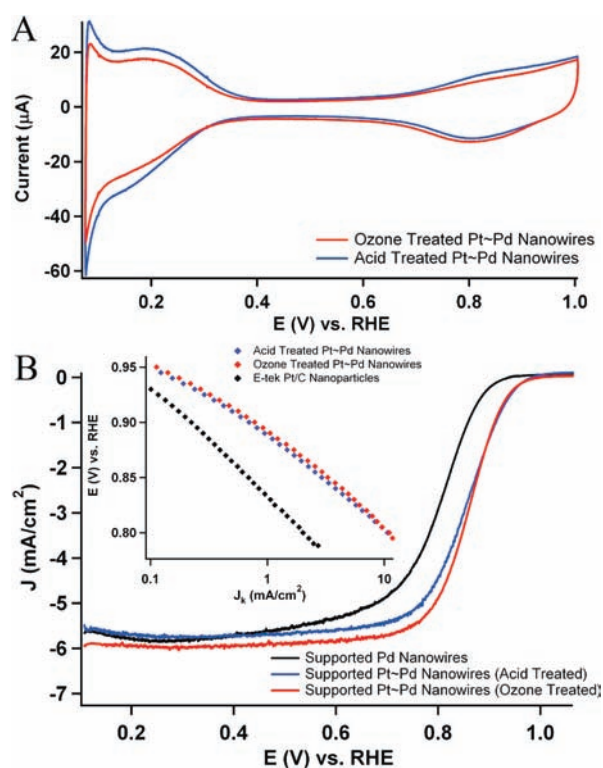
Figure 5. Cyclic voltammograms (A) obtained for the ozone and acid-treated Pt−Pd NW/C core−shell nanowires, after Pt monolayer deposition, loaded separately onto a GCE in a 0.1 M HClO$_4$ solution at 20 mV/s. (B) The polarization curves for the treated Pt−Pd/C core−shell nanowire composites were both obtained on a glassy carbon rotating disk electrode. Curves (anodic sweep direction) were collected using a rotation rate of 1600 rpm in a 0.1 M HClO$_4$ solution at 20 °C. Kinetic current vs potential plots (inset) of treated Pt−Pd/C composites and commercial carbon supported Pt nanoparticles are also presented.

Pt nanowires demonstrated significantly enhanced activities as a result of their uniquely advantageous surface structure. Similarly, Abruña and co-workers have also shown that 1D structures of Pd preferentially display certain low energy crystal facets, which are inherently highly active toward ORR.[25]

In this case, these Pd nanowires are analogous to our platinum nanowires and are also composed of single crystalline segments, which are believed to maintain fewer defect sites. It has been previously observed that the use of basic amine-terminated surfactants results in the preferential growth along the ⟨111⟩ crystallographic direction as a result of selective adsorption to the (100) facets.[60] Thus, it is not surprising that the use of octadecylamine[38] (a basic surfactant) results in preferential growth along the ⟨111⟩ direction (Figure 1D), thereby suggesting the presence of low energy facets.

In addition, the H$_{ads}$ profile of the Pd NW/C composites in Figure 2 is unique when compared with that of the Pd NP/C catalyst. Specifically, the CV of the Pd NP/C displays two broad peaks centered at approximately 0.27 and 0.20 V in the anodic sweep segment, respectively, whereas the Pd NW/C CV shows only a single peak centered at 0.27 V with a corresponding shoulder at 0.20 V. The presence of fewer peaks in the H$_{ads}$ region may suggest a more uniform surface. However, it is very difficult to evaluate the H$_{ads}$ profile in nanostructured palladium, because hydrogen adsorption is overshadowed by hydrogen
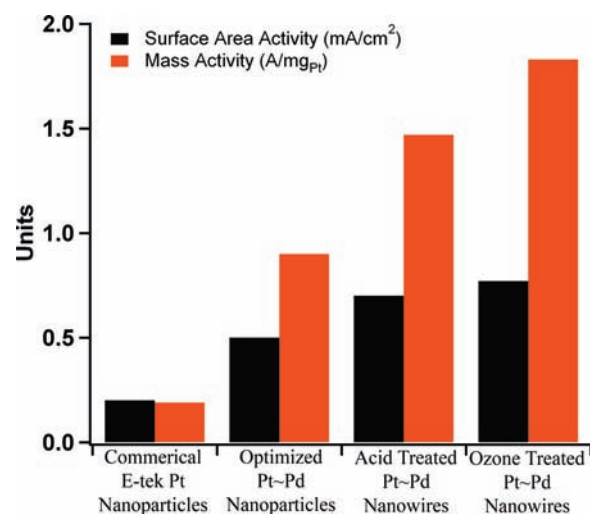
absorption on well-defined Pd single crystals. Hence, we believe that the Pd NW/C nanostructures possess more uniform defect free surfaces resulting in a suppression of the cathodic overpotential and a corresponding increase in the ORR activity, based on previous results from analogous ultrathin nanowires and the analysis of our Pd NW/C composites. Although it is beyond the scope of this study, further exploration of the origin of this enhancement is necessary to fully understand the activity of these composites. Nonetheless, the observed structure-dependent enhancement confirms that the ultrathin Pd NWs should be a superior substrate for Pt monolayer deposition.

3.4. Structure-Dependent ORR Activity in Pd NW Core−Pt Monolayer Shell Composites. The deposition of a monolayer quantity of platinum onto the surface of the treated Pd NW/C composites was achieved by Cu UPD followed by galvanic displacement of the Cu adatoms with Pt^{2+}. Cyclic voltammetry of the resulting Pt monolayer shell−Pd NW/C core (Pt−Pd NW/C) (Figure 5A) showed (i) a H$_{ads}$ region that resembled that of the platinum (111) surface and (ii) a delay in the oxidation and the reduction of the surface to higher potentials, when compared with the Pd NW/C composite. These results are in excellent agreement with those from previous reports of platinum monolayers deposited onto Pd single crystals[27] and, more importantly, elemental[30] and alloyed[29,32] palladium nanoparticles. On the basis of a previous study of Pt monolayer deposition on Pd (111) single crystals, the surface is found to be composed of interconnected Pt islands with some regions of bare Pd surface exposed.[30] It is important to highlight that the Cu UPD charge is in excellent agreement with the H$_{ads}$ charge obtained after monolayer deposition, confirming the near monolayer deposition of Pt. Although it is beyond the scope of this report, the structure of the Pt monolayer will be explored as a function of morphology in future reports.

The ORR activity of the Pt−Pd NW/C composites was measured electrochemically by obtaining polarization curves in oxygen-saturated 0.1 M HClO$_4$ (Figure 5B) solution. Both the acid- and ozone-treated nanowires displayed an ORR onset in the region of 0.9−1.0 V, which is consistent with that of nanostructured Pt catalysts. In addition, the core−shell nanowires

composites displayed dramatically enhanced ORR activity as compared with the Pd NW/C catalyst before Cu UPD, which is shown in Figure 5B for clarity. This observation further confirms the successful deposition of a platinum monolayer atop the Pd NW substrate. In order to probe the intrinsic activity of the core—shell nanowires, the measured kinetic currents at 0.9 V were normalized to the electrochemical surface areas, as determined from the hydrogen adsorption charge obtained from the composite structure. Similarly, the platinum mass activity was deduced by normalizing the measured kinetic current to the mass of Pt deposited, which can be readily extracted from the Cu UPD voltammograms (Figure S6, Supporting Information).

The area- and mass-specific activities of the treated core—shell nanowires are summarized in Figure 6 by comparison with commercial platinum nanoparticles and optimized Pt—Pd core—shell nanoparticles[32] prepared analogously. The ozone-treated nanowires maintained outstanding area-specific and mass-specific activities of 0.77 mA/cm^2 and 1.83 A/mg$_{Pt}$, respectively. By comparison, the acid-treated nanowires also demonstrated high area- and mass-specific activities of 0.70 mA/cm^2 and 1.47 A/mg$_{Pt}$, which were, however, noticeably lower in magnitude as compared with that of ozone-treated nanowires. The exceptional enhancement in the activity of the ozone-treated nanowires again highlights the dependence of the treatment method upon the inevitable activity of nanowire catalysts. The structure of the polarization curve in the mixed control region indicates that the ozone-treated nanowires maintain an improved dispersion on the carbon surface as well as less aggregation. This observation readily explains the significant difference in mass specific activity, which is dependent upon the dispersion of the catalyst and the degree of aggregation, whereas there is little difference in the area-specific activity, which is more closely related to the intrinsic active sites of the catalyst.[28]

Nonetheless, both core—shell nanowire systems maintain significantly enhanced activities when compared with commercial Pt nanoparticles and optimized core—shell nanoparticles. Although the as-obtained activities greatly exceed the mass activity target of 0.44 A/mg$_{Pt}$ projected for 2015 by the DOE, further testing under MEA conditions is required in order to fully understand the potential of these catalysts.[26] However, care must be taken when comparing the values obtained herein and the reported targets, because RDE methods yield comparable but not necessarily identical activity results to those acquired under actual MEA conditions. To highlight the outstanding activity of the core—shell nanowires, a plot of the kinetic current vs the potential (inset to Figure 5B) demonstrably reveals that the core—shell nanowires maintain higher kinetic currents over the entire range of plausible operating potentials as compared with commercial Pt nanoparticles.

Although it is not surprising that the activity of core—shell nanowire systems greatly exceeds that of commercial Pt nanoparticles, the nanowires display a distinctive structure-dependent enhancement as compared with analogous core—shell nanoparticles prepared from an optimized procedure by one of our groups.[32] Specifically, the ozone- and acid-treated core—shell nanowire systems display enhancements in area-specific activity of 1.54 and 1.40 fold, respectively, as well as enhancements in Pt mass-specific activity of 2.03 and 1.60 fold, respectively. Given that palladium is also considered to be a platinum group metal (PGM), the mass activity can also be reported with respect to the total PGM loading, as determined by TGA analysis. The PGM mass activity for the ozone-treated and acid-treated Pt—Pd NW/C

samples were determined to be 0.55 A/mg and 0.32 A/mg, respectively. Both of these represent a true enhancement when compared with the PGM mass activity values of 0.25 A/mg and 0.19 A/mg obtained for the analogous optimized core—shell Pt—Pd and commercial Pt nanoparticles, respectively.

We attribute the enhancement in the activity of our ultrathin nanowires to a reconstruction of the nanowire surface that increases the strain-induced contraction of the Pt monolayer. Recently, several theoretical[35,36] and experimental[37] studies have shown that metallic nanowires composed of platinum group metals (e.g., Au, Pt, Ir) undergo a distinctive surface contraction, when their diameter is decreased below a critical value of approximately 2—4 nm. A contraction of the core nanowire surface would inherently result in an enhancement in the strain-induced compression of the Pt monolayer shell, thereby causing a decrease in OH adsorption and a corresponding increase in ORR kinetics.[28,32,33] The same effect has been achieved in Pd nanoparticles alloyed with certain third-row transition metals and recently in more elegant transition metal core—noble metal shell nanoparticles, wherein the surface of the Pd is contracted by the presence of transition metals with smaller atomic radii.[29,61—64] However, the incorporation of less noble transition metals can lead to an inevitable increase in corrosion processes under operating conditions, which can compromise the durability of these nanostructures for long-term use in fuel cells.[65] Thus, we believe that the uniquely advantageous properties of ultrathin nanowires can allow for the enhancement of Pt monolayer activity by increased strain-induced effects without the need for additional third row transition metal dopants and without potentially compromising the durability of the resulting core—shell composite. As expected, the ultrathin Pd NW core—Pt monolayer shell composites (Figure 6) displayed outstanding durability in an accelerated half cell test, an observation which is discussed in detail in the next section.

3.5. Accelerated Durability Testing of Treated Pd Nanowire Core—Pt Monolayer Shell Composites. The electrochemical durability of the ozone-treated Pt—Pd NW/C composites was studied under half-cell conditions. In this report, we have elected to apply an accelerated durability test outlined by the DOE for catalysts under MEA conditions.[26] Specifically, the potential was cycled between 0.6 and 1.0 V so as to bracket the relevant potential region wherein ORR can feasibly occur in a working fuel cell. The electrode was immersed in naturally aerated 0.1 M HClO$_4$ solution. However, we highlight that care must be taken when comparing these results to those obtained under actual MEA conditions. Hence, identical experiments were performed on high performance Pt nanoparticle catalysts supported on carbon, which are the most commonly utilized catalysts associated with commercial fuel cells, for the purposes of comparison.

Upon the basis of this protocol, the ESA and the ECSA could be independently probed by obtaining cyclic voltammograms (Figure 7A and 7C) and polarization curves (Figure 7B and D), respectively, over the course of an accelerated catalyst lifetime (30 000 cycles). After an accelerated lifetime, the ozone-treated Pt—Pd NW/C composites maintained 63% of their initial measured ESA. By contrast, the commercial HP Pt nanoparticulate catalysts maintained only slightly more than 50% of the initial measured ESA. As expected, the ESA of the PtNP catalysts rapidly decreases to ~50% over the first 15 000 cycles, inevitably reaching a steady state. The rapid decline in ESA observed with nanoparticle catalysts can be attributed to the rapid agglomeration, dissolution, and ripening of the nanoparticles under
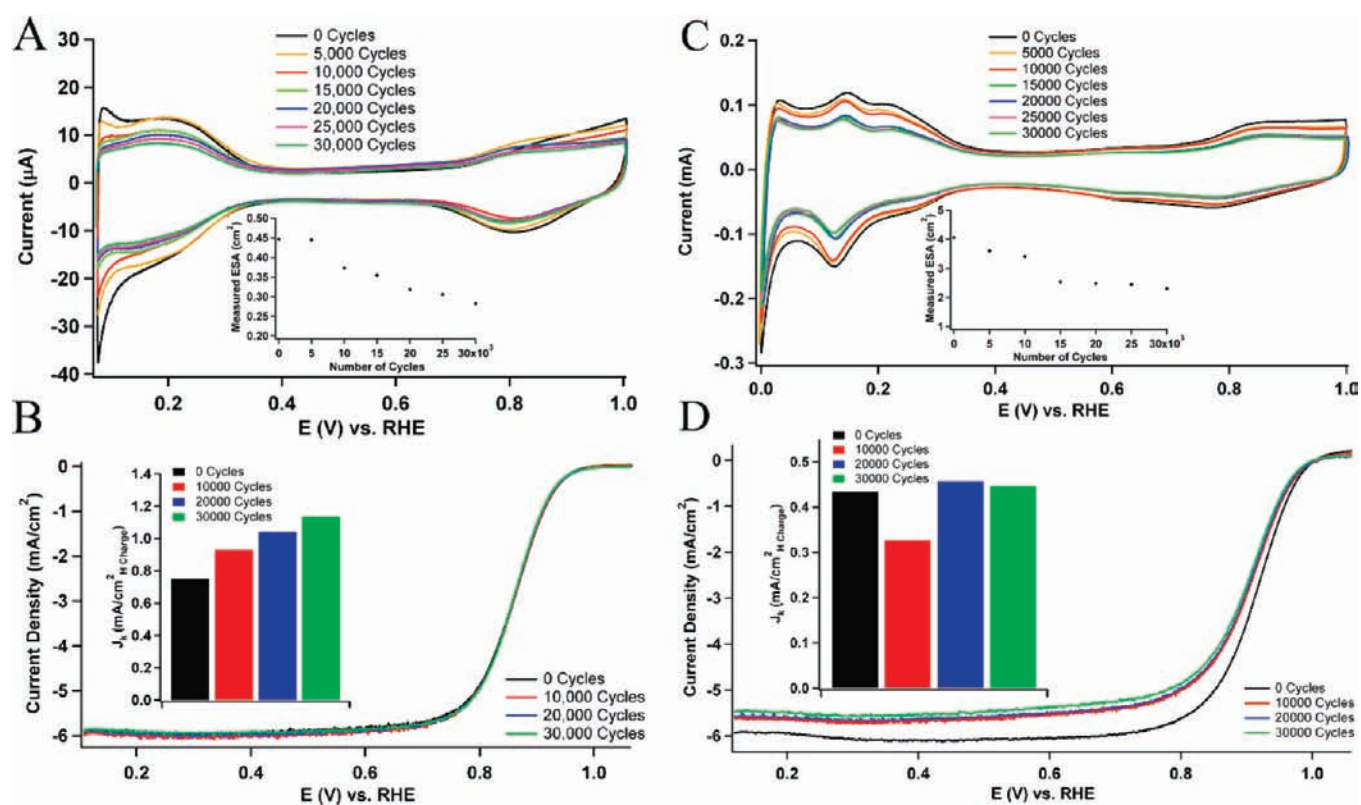
9792

dx.doi.org/10.1021/ja111130t |*J. Am. Chem. Soc.* 2011, 133, 9783–9795

Figure 7. Cyclic voltammograms obtained in deoxygenated 0.1 M HClO$_4$ solution after 5000 cycles for the Pt−Pd NW/C core shell composites (A) and commercial high performance (HP) Pt/C catalysts (C). The measured ESA loss is also shown as a function of durability cycling for the Pt−Pd NW/C composites and HP Pt/C catalysts as insets to A and C, respectively. The polarization curves (anodic sweep direction) obtained in an oxygen saturated 0.1 M HClO$_4$ solution at 1600 rpm after 10 000 cycles for the Pt−Pd NW/C composites (B) and the HP Pt/C catalysts (D) are presented. Measured area-specific kinetic currents (ECSA) are also shown as a function of durability cycling for the Pt−Pd NW/C composites and the HP Pt/C composites as insets to B and D, respectively.

operating potentials.[11] However, the core−shell nanowires displayed a more linear decline in the ESA, and by 15 000 cycles, our nanowires still retained more than 80% of their original ESA. The steady decline in ESA in Pt−Pd core−shell catalysts has been attributed to the preferential dissolution of Pd from the catalyst core and is supporting proof that the nanowire morphology does not undergo either significant aggregation or ripening.[66] A representative TEM image of ozone-treated Pt−Pd NW samples after 30 000 cycles is shown in Figure S8, Supporting Information. As expected, the long nanowires have been converted largely into wire fragments with lengths that are commensurate with the single crystalline segments present in the initial long nanowires. Upon the basis of the fragmentation pattern of the nanowires, the loss of ESA can be attributed largely to the preferential dissolution of the nanowires at the interconnects between the single crystalline segments and to the concomitant formation of some nanoparticles.

In addition to monitoring the ESA, the surface area activity of the ozone-treated Pt−Pd NW/C composites and commercial nanoparticles was also studied over the course of a catalyst lifetime. Interestingly, the ozone-treated area-specific activity of the ozone-treated Pt−Pd NW/C composites *increases* by more than 1.5 fold over the course of the accelerated test, despite nearly a 40% loss in ESA. In fact, there is no substantial change either in the half wave potential (i.e., 3 mV loss after 30 000 cycles) or in the diffusion current of the polarization curve even after 30 000 cycles, which suggests that there is no overall loss in activity from the electrode. The enhancement in surface area activity in core−shell catalysts

has recently been studied under MEA conditions by one of our groups, and the results are in excellent agreement with these prior data.[66] It is believed that the preferential dissolution of Pd from the core in combination with a restructuring of the platinum monolayer mutually contribute to enhance the performance of the catalyst and to prevent corrosion of the Pt monolayer.

By contrast, the surface area activity of the commercial HP Pt nanoparticles remains essentially unchanged after 30 000 cycles. However, it is important to highlight that there is a substantial activity loss of greater than 25% during the first 5000 and 10 000 cycles, which coincides with the rapid decline in the ESA of the nanoparticles and is consistent with a restructuring of the catalyst. The polarization curves show a significant decline in the half wave potential of 15 mV and an associated decrease in the diffusion limited current. Hence, as-prepared core−shell nanowire catalysts maintain far superior durability in terms of both resistance to surface area loss and, more importantly, activity loss when compared with commercial Pt nanoparticle catalysts. However, fuel cell testing under MEA conditions will be required in the future in order to further understand the durability of these novel one-dimensional nanostructures and to quantitatively compare their durability with that of core−shell nanoparticles.

To explore the dependence of treatment upon the durability of the resulting core−shell nanowire catalyst, we probed the corresponding durability of the acid-treated core−shell nanowires (Figure S7, Supporting Information) utilizing an identical procedure. In this case, the acid-treated nanowires were tested

until a steady state was achieved in both ESA and surface area activity after 20 000 cycles. After 20 000 cycles, the acid-treated nanowires maintained 63% of their initial ESA, which was significantly lower than that of the ozone-treated nanowires (71%). Acid-treated nanowires also showed no significant enhancement in activity over the 20 000 cycles, whereas the ozone-treated nanowires maintained an enhancement of 1.4 fold after 20 000 cycles. Thus, ozone-treated nanowires displayed enhanced electrochemical durability as compared with acid-treated nanowires, an observation which is consistent with both the electron microscopy and the electrochemical activity results.

4. CONCLUSIONS

In this report, we have synthesized crystalline Pd nanowires with a diameter of 2.0 ± 0.5 nm and reliably supported them onto carbon with a highly uniform catalyst distribution. As-prepared nanowires were treated with either UV-generated ozone or glacial acetic acid, followed by selective CO adsorption in order to remove the residual, undesirable organic residue. Upon the basis of electron microscopy and electrochemical measurements, it was determined that the ozone treatment results in nanowires that possess higher activity and durability as compared with acid-treated nanowires, an observation attributable to the retention of morphology and dispersion upon ozone treatment. After activation, the structure-dependent activity of the Pd NW/C composites was studied by comparison with commercial Pd nanoparticles; it was found that the ozone-treated nanowires maintained an enhanced area-specific activity that was more than double that of the commercial nanoparticles. Subsequently, the desired nanowire core—Pt monolayer shell motif was achieved by Cu UPD followed by galvanic displacement of the Cu adatoms with Pt^{2+}; the deposition process was confirmed by both cyclic voltammetry and ORR activity data.

The surface area and mass activity of the acid- and ozone-treated nanowires were explored with respect to commercial Pt nanoparticles and optimized core—shell Pt—Pd nanoparticles. Ozone-treated nanowires were found to maintain outstanding area and mass specific activities of 0.77 mA/cm^2 and 1.83 A/mg, respectively, which were significantly enhanced as compared with commercial Pt nanoparticles, core—shell nanoparticles, and acid-treated nanowires. Ozone-treated nanowires also maintained excellent electrochemical durability under accelerated half-cell testing, and it was found that the area-specific activity increased by 1.5 fold after a simulated lifetime.

■ ASSOCIATED CONTENT

ⓢ Supporting Information. Figures, experimental protocols, and additional diffraction, electron microscopy, and electrochemical data for the characterization of our nanostructures. This material is available free of charge via the Internet at http://pubs.acs.org.

■ AUTHOR INFORMATION

Corresponding Author
sswong@notes.cc.sunysb.edu; sswong@bnl.gov; adzic@bnl.gov

■ ACKNOWLEDGMENT

■ REFERENCES

(1) *Fuel cell catalysts*; Koper, M. T. M., Ed.; Wiley Interscience: Hoboken, NJ, 2009.

(2) Lamy, C. In *Carbons for electrochemical energy storage and conversion systems*; 1st ed.; Beguin, F., Frackowiak, E., Eds.; CRC Press: Boca Raton, FL, 2010; pp 377—409.

(3) Norskov, J. K.; Rossmeisl, J.; Logadottir, A.; Lindqvist, L.; Kitchin, J. R.; Bligaard, T.; Jonsson, H. *J. Phys. Chem. B* **2004**, *108*, 17886–17892.

(4) Wang, J. X.; Zhang, J.; Adzic, R. R. *J. Phys. Chem. A* **2007**, *111*, 12702–12710.

(5) He, C.; Desai, S.; Brown, G.; Bollepalli, S. *Electrochem. Soc. Interface* **2005**, *14*, 41–44.

(6) Gewirth, A. A.; Thorum, M. S. *Inorg. Chem.* **2010**, *49*, 3557–3566.

(7) Yu, X.; Ye, S. *J. Power Sources* **2007**, *172*, 145–154.

(8) Williams, M. C. *Fuel Cells* **2001**, *1*, 87–91.

(9) Markovic, N. M.; Ross, P. N. In *Interfacial Electrochemistry: Theory, Experiment and Applications*; Wieckowski, A., Ed.; Marcel Dekker, Inc: New York, 1999; Vol. 1, pp 821—841.

(10) Markovic, N. M.; Schmidt, T. J.; Stamenkovic, V.; Ross, P. N. *Fuel Cells* **2001**, *1*, 105–116.

(11) Shao, Y.; Yin, G.; Gao, Y. *J. Power Sources* **2007**, *171*, 558–566.

(12) Sinha, J.; Marcinkoski, J.; Randolph, K.; Benjamin, T. G. *Cost Analysis of Fuel Cell Stacks/Systems*, DOE Hydrogen Program Review, 2009.

(13) Koenigsmann, C.; Wong, S. S. *Energy Environ. Sci.* **2011**, *4*, 1161–1176.

(14) Xia, Y.; Yang, P.; Sun, Y.; Wu, Y.; Mayers, B.; Gates, G.; Yin, Y.; Kim, F.; Yan, H. *Adv. Mater.* **2003**, *15*, 353–389.

(15) Cademartiri, L.; Ozin, G. A. *Adv. Mater.* **2009**, *21*, 1013–1020.

(16) Subhramannia, M.; Pillai, V. K. *J. Mater. Chem.* **2008**, *18*, 5858–5870.

(17) Wang, C.; Waje, M.; Wang, X.; Tang, J. M.; Haddon, R. C.; Yan *Nano Lett.* **2003**, *4*, 345–348.

(18) Chen, Z.; Waje, M.; Li, W.; Yan, Y. *Angew. Chem., Int. Ed.* **2007**, *46*, 4060–4063.

(19) Koenigsmann, C.; Zhou, W.-p.; Adzic, R. R.; Sutter, E.; Wong, S. S. *Nano Lett.* **2010**, *10*, 2806–2811.

(20) Lim, B.; Jiang, M.; Camargo, P. H. C.; Cho, E. C.; Tao, J.; Lu, X.; Zhu, Y.; Xia, Y. *Science* **2009**, *324*, 1302–1305.

(21) Sun, S.; Jaouen, F.; Dodelet, J.-P. *Adv. Mater.* **2008**, *20*, 3900–3904.

(22) Wang, D.; Luo, H.; Kou, R.; Gil, M. P.; Xiao, S.; Golub, V. O.; Yang, Z.; Brinker, C. J.; Lu, Y. *Angew. Chem., Int. Ed.* **2004**, *43*, 6169–6173.

(23) Zhou, H.; Zhou, W.-p.; Adzic, R. R.; Wong, S. S. *J. Phys. Chem. C* **2009**, *113*, 5460–5466.

(24) Tian, M.; Kumar, N.; Xu, S.; Wang, J.; Kurtz, J. S.; Chan, M. H. W. *Phys. Rev. Lett.* **2005**, *95*, 076802.

(25) Xiao, L.; Zhuang, L.; Liu, Y.; Lu, J.; Abruña, H. D. *J. Am. Chem. Soc.* **2008**, *131*, 602–608.

(26) *Multi-Year Research, Development and Demonstration Plan: Planned Program Activities for 2005—2015*, Department of Energy, 2009.

(27) Zhang, J.; Vukmirovic, M. B.; Xu, Y.; Mavrikakis, M.; Adzic, R. R. *Angew. Chem., Int. Ed.* **2005**, *44*, 2132–2135.

(28) Adzic, R.; Zhang, J.; Sasaki, K.; Vukmirovic, M.; Shao, M.; Wang, J.; Nilekar, A.; Mavrikakis, M.; Valerio, J.; Uribe, F. *Top. Catal.* **2007**, *46*, 249–262.

(29) Zhang, J.; Lima, F. H. B.; Shao, M. H.; Sasaki, K.; Wang, J. X.; Hanson, J.; Adzic, R. R. *J. Phys. Chem. B* **2005**, *109*, 22701–22704.

(30) Zhang, J.; Mo, Y.; Vukmirovic, M. B.; Klie, R.; Sasaki, K.; Adzic, R. R. *J. Phys. Chem. B* **2004**, *108*, 10955–10964.

(31) Brankovic, S. R.; Wang, J. X.; Adzic, R. R. *Surf. Sci.* **2001**, *474*, L173–L179.

(32) Wang, J. X.; Inada, H.; Wu, L.; Zhu, Y.; Choi, Y.; Liu, P.; Zhou, W.-P.; Adzic, R. R. *J. Am. Chem. Soc.* **2009**, *131*, 17298–17302.

(33) Rossmeisl, J.; Nørskov, J. K. *Surf. Sci.* **2008**, *602*, 2337–2338.

(34) Greeley, J.; Nørskov, J. K. *J. Phys. Chem. C* **2009**, *113*, 4932–4939.

(35) Haftel, M. I.; Gall, K. *Phys. Rev. B: Condens. Matter* **2006**, *74*, 035420–035412.

(36) Diao, J.; Gall, K.; Dunn, M. L. *Nat. Mater.* **2003**, *2*, 656–660.

(37) Kondo, Y.; Takayanagi, K. *Science* **2000**, *289*, 606–608.

(38) Teng, X.; Han, W.; Ku, W.; Hucker, M. *Angew. Chem., Int. Ed.* **2008**, *47*, 2055–2058.

(39) Mazumder, V.; Sun, S. *J. Am. Chem. Soc.* **2009**, *131*, 4588–4589.

(40) Garsany, Y.; Baturina, O. A.; Swider-Lyons, K. E.; Kocha, S. S. *Anal. Chem.* **2010**, *82*, 6321–6328.

(41) Dean, J. A. *Lange's Handbook of Chemistry*, 14th ed.; McGraw-Hill: New York, 1992.

(42) Yu, X.; Ye, S. *J. Power Sources* **2007**, *172*, 133–144.

(43) Dicks, A. L. *J. Power Sources* **2006**, *156*, 128–141.

(44) Wang, C.; Daimon, H.; Onodera, T.; Koda, T.; Sun, S. *Angew. Chem., Int. Ed.* **2008**, *47*, 3588–3591.

(45) Gonzalez, S.; Illas, F. *Surf. Sci.* **2005**, *598*, 144–155.

(46) Kato, H. S.; Okuyama, H.; Yoshinobu, J.; Kawai, M. *Surf. Sci.* **2002**, *513*, 239–248.

(47) Li, Y.; El-Sayed, M. A. *J. Phys. Chem. B* **2001**, *105*, 8938–8943.

(48) Hiura, H.; Ebbesen, T. W.; Tanigaki, K. *Adv. Mater.* **1995**, *7*, 275–276.

(49) Ranpura, H. M.; Butler, D. H.; Chang, L. H.; Tracy, C. J.; Beaudoin, S. P. *J. Electrochem. Soc.* **1999**, *146*, 3114–3118.

(50) Aliaga, C.; Park, J. Y.; Yamada, Y.; Lee, H. S.; Tsung, C.-K.; Yang, P.; Somorjai, G. A. *J. Phys. Chem. C* **2009**, *113*, 6150–6155.

(51) Pang, S.; Kurosawa, Y.; Kondo, T.; Kawai, T. *Chem. Lett.* **2005**, *34*, 544–545.

(52) Tanuma, T.; Terazono, S. *J. Power Sources* **2008**, *181*, 287–291.

(53) Prabhuram, J.; Wang, X.; Hui, C. L.; Hsing, I. M. *J. Phys. Chem. B* **2003**, *107*, 11057–11064.

(54) Park, J.; Aliaga, C.; Renzas, J.; Lee, H.; Somorjai, G. *Catal. Lett.* **2009**, *129*, 1–6.

(55) Chen, W.; Kim, J.; Sun, S.; Chen, S. *Phys. Chem. Chem. Phys.* **2006**, *8*, 2779–2786.

(56) Liu, Z.; Shamsuzzoha, M.; Ada, E. T.; Reichert, W. M.; Nikles, D. E. *J. Power Sources* **2007**, *164*, 472–480.

(57) Mazumder, V.; Lee, Y.; Sun, S. *Adv. Funct. Mater.* **2010**, *20*, 1224–1231.

(58) Kobayashi, H.; Yamauchi, M.; Kitagawa, H.; Kubota, Y.; Kato, K.; Takata, M. *J. Am. Chem. Soc.* **2008**, *130*, 1828–1829.

(59) Martín, A. J.; Chaparro, A. M.; Folgado, M. A.; Rubio, J.; Daza, L. *Electrochim. Acta* **2009**, *54*, 2209–2217.

(60) Teng, X.; Yang, H. *Nano Lett.* **2005**, *5*, 885–891.

(61) Zhang, J.; Vukmirovic, M. B.; Sasaki, K.; Nilekar, A. U.; Mavrikakis, M.; Adzic, R. R. *J. Am. Chem. Soc.* **2005**, *127*, 12480–12481.

(62) Gong, K.; Chen, W.-F.; Sasaki, K.; Su, D.; Vukmirovic, M. B.; Zhou, W.-p.; Izzo, E. L.; Perez-Acosta, C.; Hirunsit, P.; Balbuena, P. B.; Adzic, R. R. *J. Electroanal. Chem.* **2010**, *649*, 232–237.

(63) Ghosh, T.; Vukmirovic, M. B.; DiSalvo, F. J.; Adzic, R. R. *J. Am. Chem. Soc.* **2010**, *132*, 906–907.

(64) Knupp, S.; Vukmirovic, M.; Haldar, P.; Herron, J.; Mavrikakis, M.; Adzic, R. *Electrocatalysis* **2010**, *1*, 213–223.

(65) Antolini, E. *Energy Environ. Sci.* **2009**, *2*, 915–931.

(66) Sasaki, K.; Naohara, H.; Cai, Y.; Choi, Y. M.; Liu, P.; Vukmirovic, M. B.; Wang, J. X.; Adzic, R. R. *Angew. Chem., Int. Ed.* **2010**, *49*, 8602–8607.